buildings

MDPI

Article

Adding Glass Fibers to 3D Printable Mortar: Effects on Printability and Material Anisotropy

Leo Gu Li [1,*], Bo-Feng Xiao [2], Cong-Mi Cheng [1,*], Hui-Zhu Xie [3] and Albert Kwok Hung Kwan [4]

[1] School of Civil Engineering, Guangzhou University, Guangzhou 510006, China
[2] Guangzhou KEO Information Technology Co., Ltd., Guangzhou 510000, China
[3] School of Civil and Transportation Engineering, Guangdong University of Technology, Guangzhou 510006, China
[4] Department of Civil Engineering, The University of Hong Kong, Hong Kong 999077, China
* Correspondence: liguleo@gzhu.edu.cn (L.G.L.); ccm@gzhu.edu.cn (C.-M.C.)

Abstract: Adding fibers is an effective way to enhance the printability and mechanical performance of 3D printable cementitious materials. Glass fibers are commonly used owing to their sound mechanical properties, high durability and affordable price. However, there is still a lack of systematic and in-depth research on the effects of adding glass fibers to cementitious materials. In this study, a series of 3D printable mortars with varying glass fiber content and water/cement (W/C) ratio were produced to evaluate their printability, flexural strength and compressive strength. The results showed that decreasing the W/C ratio generally has positive effects on printability and mechanical performance, whereas increasing the glass fiber content from 0% to 1% would substantially improve the extrudability, dimensional stability and buildability; increase the flexural strength by up to 82%; but decrease the compressive strength by up to 35%. Such large differences in the effects of glass fibers on the flexural and compressive strengths indicate significant material anisotropy. In fact, comparison of the strength results of printed specimens to those of un-printed specimens reveals that the printing process could increase the flexural strength by 98% but decrease the compressive strength by 47%.

Keywords: 3D printing; glass fibers; printability; printable mortar; material anisotropy due to printing

check for updates

Citation: Li, L.G.; Xiao, B.-F.; Cheng, C.-M.; Xie, H.-Z.; Kwan, A.K.H. Adding Glass Fibers to 3D Printable Mortar: Effects on Printability and Material Anisotropy. *Buildings* **2023**, *13*, 2295. https://doi.org/10.3390/buildings13092295

Academic Editor: Chang-Su Shim

Received: 7 August 2023
Revised: 30 August 2023
Accepted: 4 September 2023
Published: 9 September 2023

Copyright: © 2023 by the authors. Licensee MDPI, Basel, Switzerland. This article is an open access article distributed under the terms and conditions of the Creative Commons Attribution (CC BY) license (https://creativecommons.org/licenses/by/4.0/).

1. Introduction

Three-dimensional concrete printing technology (3D-CPT) is a novel and promising construction technology which shows great potential to proliferate the industrialization and intellectualization of building construction [1–3]. In recent years, 3D-CPT is rapidly gaining ground in some applications [4–6]. Nevertheless, compared to conventional concrete construction methods, it is obvious that the absence of effective reinforcement is a detrimental weakness of 3D printed concrete. Applying reinforcing fibers to improve the tensile strength and toughness of 3D printed concrete is undoubtedly one of the effective ways of providing reinforcement [7–10].

Reinforcing fibers play an important role in the mechanical performance of 3D printed concrete, especially the flexural/tensile strength of the concrete, but the actual performance has an element of mechanical anisotropy [11–15]. Hambach and Volkmer [16] demonstrated that the extrusion process would align the fibers to be along the printing path, leading to an improvement in flexural/tensile strength of the printed mortar in the direction of printing. Bos et al. [17] revealed that the toughness of 3D printed mortar reinforced with short straight steel fibers is much higher than that of plain mortar without fibers. Panda et al. [18] made 3D printed mortar added with glass fibers, and tested that the flexural, tensile and compressive strengths in different loading directions are widely different, indicating that the layer-by-layer deposition could cause significant material anisotropy. Ma et al. [19] produced polypropylene (PP)-fiber-reinforced 3D printed mortar and observed that the tensile stresses perpendicular

to the interlayer zones between adjacent layers tended to induce cracks more readily than those parallel to the interlayer zones. Liu et al. [20] prepared polyvinyl alcohol (PVA)-fiber-reinforced 3D printed mortar and found that depending on the printing and loading directions, the strength of printed specimens could be higher or lower than the strength of just cast specimens.

The reinforcing fibers have been found to also have significant effects on the fresh properties and printability of 3D printable cementitious materials [21–23]. For instance, Rubio et al. [24] noted that adding PP fibers could boost the cohesiveness of mortar for building up a more stable structure. Van Der Putten et al. [25] reported that increasing the PP fiber dosage would reduce the workability of 3D printable mortar partly because the use of PP fibers might thin the water film thickness. Arunothayan et al. [26] found that adding 2% steel fibers would slightly decrease workability but would enhance the shape-retention ability. Shakor et al. [27] showed that the use of glass fibers would allow the printable mortar to be printed at higher speed without causing negative effects. Weng et al. [28] revealed that increasing the PVA fiber content would increase the flow resistance, torque viscosity and thixotropy of the printable mortar mix; they developed some empirical models to predict these rheological properties.

Among the various fibers, glass fibers have been widely used in traditional fiber-reinforced concrete [29–31] and also tried in 3D-CPT [18,27,32]. However, there is still a lack of systematic and in-depth research on how glass fibers would affect the printability and mechanical properties of 3D printable cementitious materials. For the purposes of evaluating the printability and mechanical properties of glass-fiber-reinforced 3D printable mortar and studying the effects of the glass fiber content, a comprehensive research program has been launched, whereby a series of printable mortar mixes with different glass fiber contents and water/cement ratios were made for testing, as presented herein. It can be seen that due to the printing process, the printed mortar is highly anisotropic and the effects of glass fibers on the flexural and compressive strengths are widely different.

2. Materials and Methodology

2.1. Raw Materials

The raw materials employed in this study were cement, fine aggregate, glass fibers, water and superplasticizer (SP). The cement used was an ordinary Portland cement, which has a strength grade of 42.5R conforming to Chinese Standard GB 175-2020 [33] and has a specific gravity of 3.10. The fine aggregate used was river sand, which had a maximum particle size of 1.18 mm, specific gravity of 2.66, water absorption of 1.10% and moisture content of 0.04%. The particle size distribution of the cement was determined by laser diffraction method (applying a laser-diffraction particle size analyzer based on the light scattering principle), and the fine aggregates were measured by a mechanical sieving method (using an automatic sieving machine by means of mechanical vibrating and sieving). The particle size distributions of the cement and fine aggregate are exhibited in Figure 1 for reference.

The glass fibers used were alkali-resistant glass fibers with a specific gravity of 2.68, a fiber diameter of 16 μm and a fiber length of 10 mm. Other properties of the glass fibers are listed in Table 1, and a photograph of the glass fibers is presented in Figure 2.

Table 1. Properties of fiber.

Fiber Type	Tensile Strength (MPa)	Elastic Modulus (GPa)	Ultimate Elongation
Alkali-resistant glass fiber	1700	72	3%

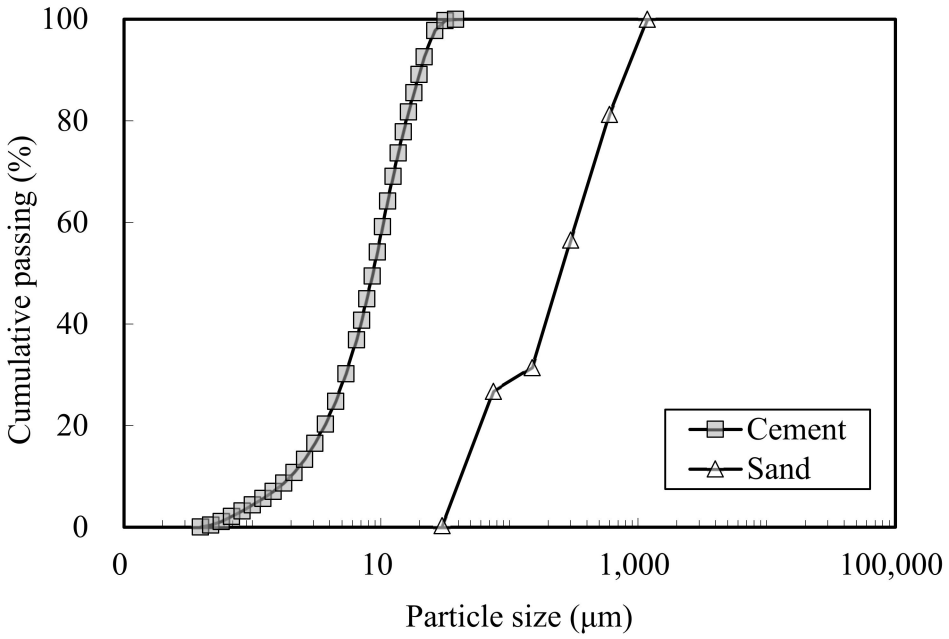


Figure 1. Grading curves of cement and sand.

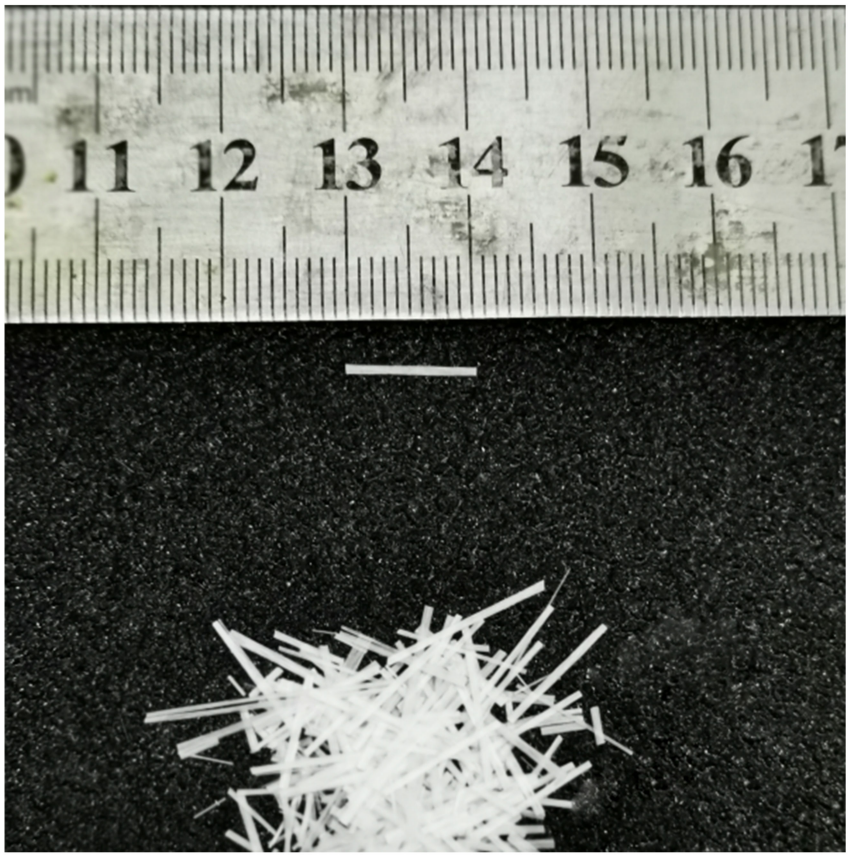


Figure 2. Photograph of glass fibers.

The water used was local tap water, and the SP used was a third-generation polycarboxylate-based admixture with a solid content of 20% and a specific gravity of 1.03.

2.2. Mixture Design

Fifteen 3D printable mortar mixtures were designed by varying the fiber content and water to cement (W/C) ratio. The fiber contents, each defined as the fiber to cement ratio

by mass, were set as either 0.00%, 0.25%, 0.50%, 0.75% or 1.00%, whereas the W/C ratios by mass were set as either 0.24, 0.28 or 0.32. For all the mortar mixtures, the cement to fine aggregate ratio by mass was fixed at 1.0. For ease of reference, each mortar mixture was assigned a mix number in the form of X–Y, in which X is the fiber content and Y is the W/C ratio, as listed in the first columns of Tables 2–4.

Table 2. Test results of fresh properties.

Mix No.	SP Dosage (%)	Flow Spread (mm)	EVC (%)	DSC (%)	BVC (%)
0.00%–0.24	0.55	185	2.10	4.57	1.07
0.00%–0.28	0.30	196	2.35	6.67	1.28
0.00%–0.32	0.10	218	2.73	14.29	1.68
0.25%–0.24	0.60	196	1.98	3.87	0.95
0.25%–0.28	0.30	197	2.04	6.12	1.27
0.25%–0.32	0.10	207	2.53	12.88	1.58
0.50%–0.24	0.65	199	1.28	3.70	0.66
0.50%–0.28	0.40	191	1.86	5.23	0.66
0.50%–0.32	0.15	211	2.67	11.54	0.76
0.75%–0.24	0.80	200	1.07	3.32	0.73
0.75%–0.28	0.40	191	1.76	5.42	0.79
0.75%–0.32	0.20	219	2.36	13.33	1.11
1.00%–0.24	0.95	190	1.08	2.94	0.47
1.00%–0.28	0.45	196	1.51	4.13	0.45
1.00%–0.32	0.30	214	2.32	11.11	0.77

Table 3. Test results of flexural strength.

Mix No.	Flexural Strength of Un-Printed Specimen (MPa)	Flexural Strength of Printed Specimen (MPa)	Change in Flexural Strength (%)
0.00%–0.24	8.70	12.24	+40.7
0.00%–0.28	8.07	10.85	+34.4
0.00%–0.32	7.90	10.70	+35.4
0.25%–0.24	9.33	15.90	+70.4
0.25%–0.28	8.70	14.86	+70.8
0.25%–0.32	8.10	12.89	+59.1
0.50%–0.24	9.20	16.55	+79.9
0.50%–0.28	8.83	15.50	+75.5
0.50%–0.32	8.00	13.00	+62.5
0.75%–0.24	9.57	18.26	+90.8
0.75%–0.28	9.20	15.81	+71.8
0.75%–0.32	8.10	13.79	+70.2
1.00%–0.24	10.77	20.90	+94.1
1.00%–0.28	10.00	19.76	+97.6
1.00%–0.32	8.37	16.10	+92.4

Table 4. Test results of compressive strength.

Mix No.	Compressive Strength of Un-Printed Specimen (MPa)	Compressive Strength of Printed Specimen (MPa)	Change in Compressive Strength (%)
0.00%–0.24	83.47	58.67	−29.7
0.00%–0.28	75.28	47.07	−37.5
0.00%–0.32	66.13	44.89	−32.1
0.25%–0.24	78.80	56.14	−28.8
0.25%–0.28	74.53	46.67	−37.4
0.25%–0.32	65.17	42.69	−34.5
0.50%–0.24	74.78	53.15	−28.9
0.50%–0.28	72.28	44.75	−38.1
0.50%–0.32	66.00	36.12	−45.3
0.75%–0.24	74.70	41.22	−44.8
0.75%–0.28	66.72	40.43	−39.4
0.75%–0.32	63.37	34.03	−46.3
1.00%–0.24	72.50	38.28	−47.2
1.00%–0.28	61.90	33.50	−45.9
1.00%–0.32	58.20	32.23	−44.6

It should be noted that a mortar mixture suitable for 3D printing needs to have a fluidity which is neither too low nor too high [34]. To ensure proper 3D printing, after numerous trials, the target range of flow spread, measured by a flow table test [35], was set within 180 to 220 mm. For the purpose of attaining this target flow spread, the optimum SP dosage (the SP dosage at which the mortar can achieve a flow spread within the above target range of 180 to 220 mm, expressed as a percentage by mass of cement) for each mortar mixture was determined by trial mortar mixing.

2.3. Flow Table Test

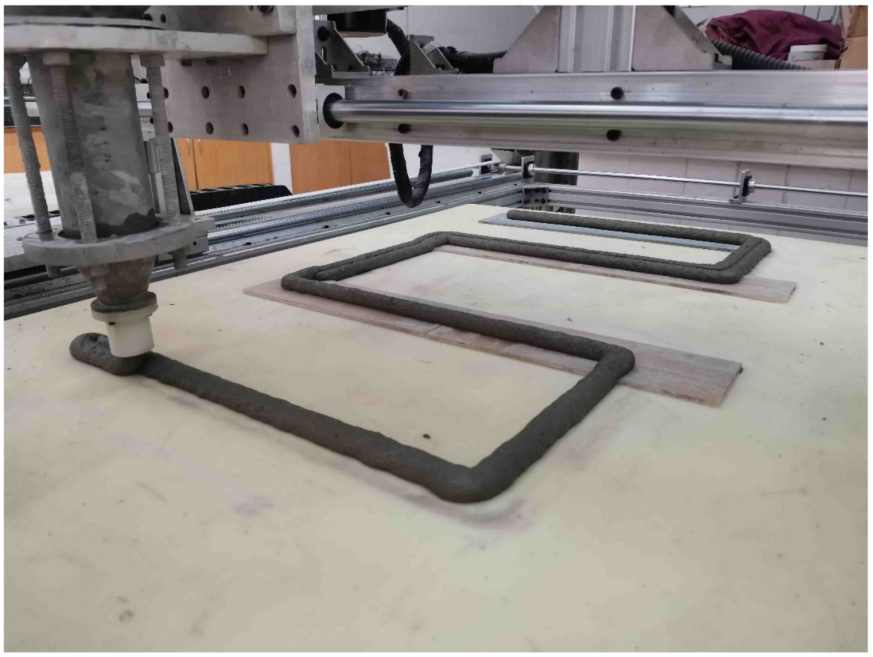
The flow table test for measuring the fluidity of the mortar mixtures in terms of flow spread followed the method specified in the Chinese Standard GB/T 2419-2005 [35]. To perform the test, the slump cone was placed on a flow table and then filled with the fresh mortar sample. Once the slump cone was full, the slump cone was lifted vertically, and the flow table was dropped 25 times in about 25 s. After dropping, the fresh mortar sample would form a patty, and the diameters of the patty in two perpendicular directions were measured. Finally, the flow spread was recorded as the average diameter of the patty, i.e., the average of the two measured diameters.

2.4. Printing Machine

As exhibited in Figure 3a, the 3D printing machine employed was a laboratory scale triaxial printer with dimensions of 2.0 m (length) × 1.6 m (width) × 1.8 m (height). The triaxial linear movement of the extruder across the printing platform was controlled by a customized computer program. The printing nozzle mounted on the extruder has a circular cross section with an internal diameter of 15 mm. The nozzle extrusion rate was set at about 9 mL/s, and the moving speed was set at about 50 mm/s. During the printing process, the fresh mortar mix was poured into the extruder and then extruded through the nozzle onto the printing platform, as shown in Figure 3b.



(a) 3D printing machine

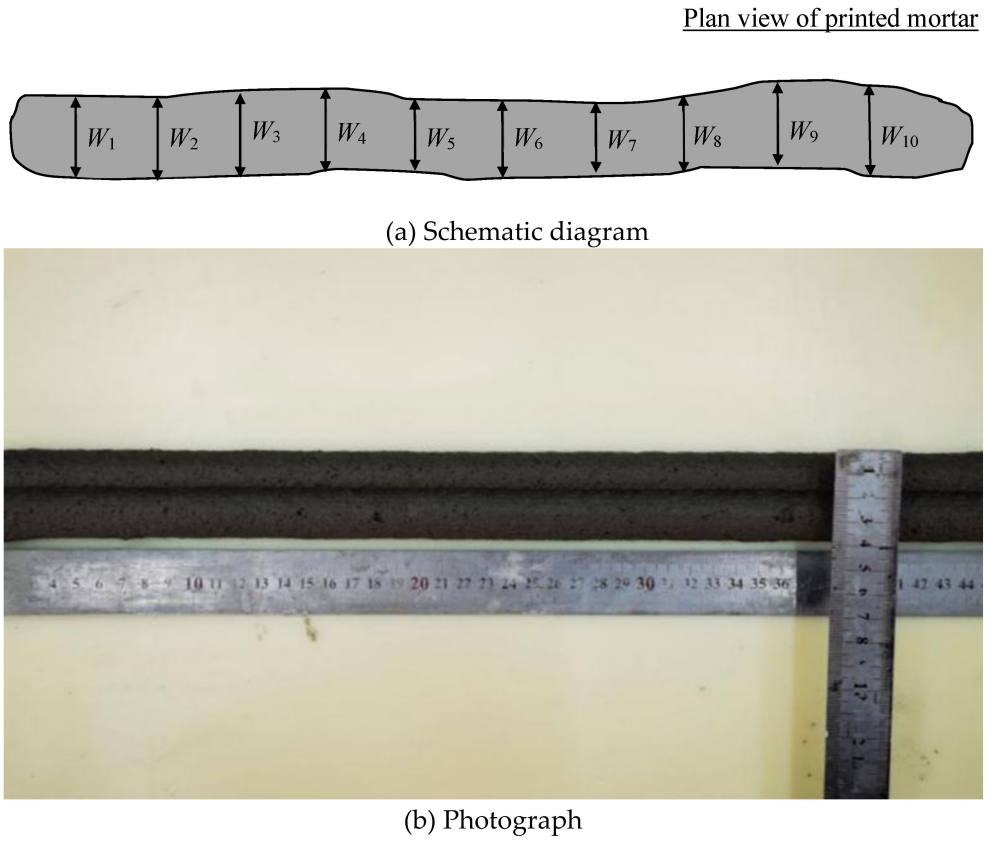


(b) Printing process

Figure 3. Photograph of 3D printing machine.

2.5. Extrudability Test

Extrudability relates to the ability of mortar to be extruded from the nozzle as a continuous and steady filament [7,36,37]. In this study, an extrudability test was applied to assess the extrudability of the fresh mortar mix for forming a single layer. For the test, two rows of mortar, each about 500 mm long, were first printed side-by-side on the printing platform. After that, the combined width *W* of the two rows of printed mortar was measured at 50 mm intervals along the length, as exhibited in Figure 4.



(a) Schematic diagram

(b) Photograph

Figure 4. Schematic diagram and photograph of extrudability test.

Based on 10 readings of combined widths, the average width and standard deviation were calculated. At the end, the extrudability variation coefficient (EVC) was determined as the standard deviation divided by the average width. A lower EVC implies better extrudability.

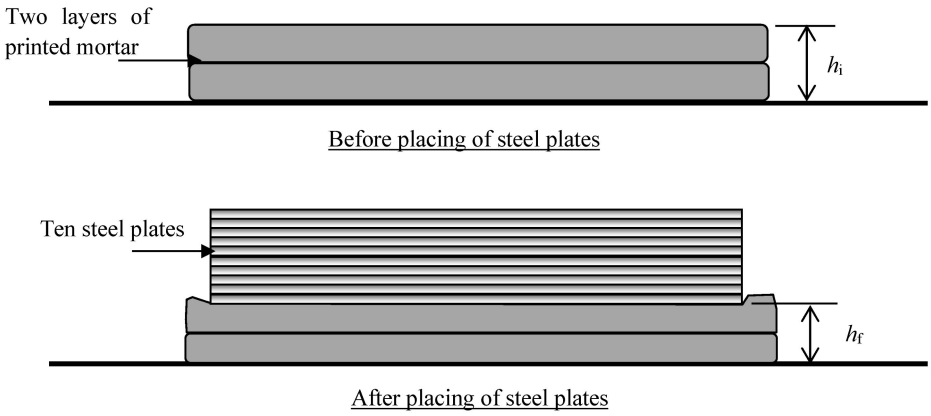
2.6. Dimensional Stability Test

Dimensional stability relates to the ability of lower layers of printed mortar to resist deformation under the weight of the upper layers during the stacking up process [38,39]. In this study, a dimensional stability test was developed by the authors' team. To perform the test, two successive layers of mortar each about 200 mm long were first printed. The total height of the printed stripe was immediately measured at 20 mm intervals. A total of 10 readings were recorded, and the initial average height h_i was calculated from the readings. Then, ten customized steel plates (each with mass equal to that of one layer of printed mortar) were placed on the printed mortar one-by-one at 30 s intervals to simulate the printing process. After that, the height of the printed mortar was recorded again to determine the final average height h_f. Finally, the dimensional stability coefficient (DSC) was determined as $(h_i - h_f)/h_i$. The lower the DSC, the better the dimensional stability. The schematic diagram and photograph of this test are displayed in Figure 5.

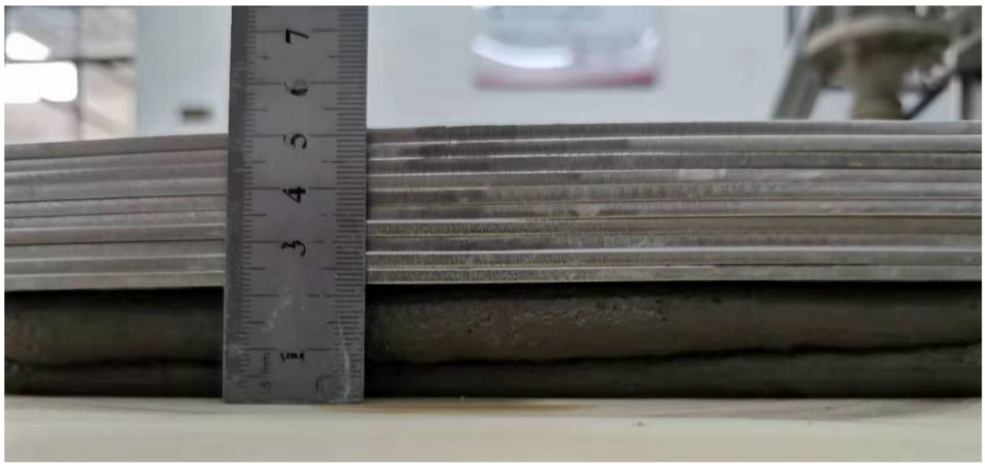
2.7. Buildability Test

Buildability relates to the ability to build up multiple layers of printed mortar continuously and steadily [40,41]. In this research, two rows of mortar each about 500 mm long were printed side-by-side, and then, additional layers were successively printed on top to build up to six layers. Afterwards, the total height H of the six layers of printed mortar at 50 mm intervals was recorded, and then, the average height and standard deviation were calculated from 10 total height readings. At the end, the buildability variation coefficient (BVC) was determined as the standard deviation divided by the average height. A lower

BVC implies better buildability. The schematic diagram and photograph of this test are displayed in Figure 6.



(a) Schematic diagram



(b) Photograph

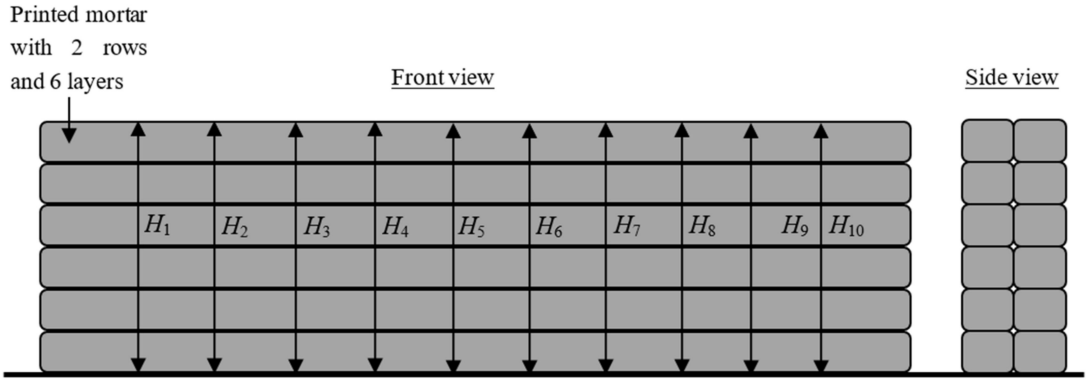
Figure 5. Schematic diagram and photograph of dimensional stability test.

2.8. Flexural Strength Test and Compressive Strength Test

To assess the flexural and compressive strengths of hardened mortar, mortar strips with two rows and three layers were first made and cured indoor by spraying water and covering plastic film at a room temperature of 20 ± 2 °C until the age of 28 days. After that, the mortar strips were cut into prismatic specimens with dimensions of 40 mm (width) × 40 mm (height) × 160 mm (length), as shown in Figure 7. All specimens were placed into a hydraulic testing machine to carry out a flexural strength test and then a compressive strength test in accordance with Chinese Standard GB/T 17671-1999 [42].

Previous studies have revealed that the printed mortar structure tends to exhibit mechanical anisotropy due to the presence of interlayer zones between adjacent layers [16–20], as shown in Figure 7.

In this study, the three-point loads for the flexural strength test and the two compression loads for the compressive strength test were applied to each prismatic specimen in the direction perpendicular to the interlayer zones to simulate the actual in-situ condition of vertical loads acting on the printed concrete structure, as shown in Figure 8.



(a) Schematic diagram

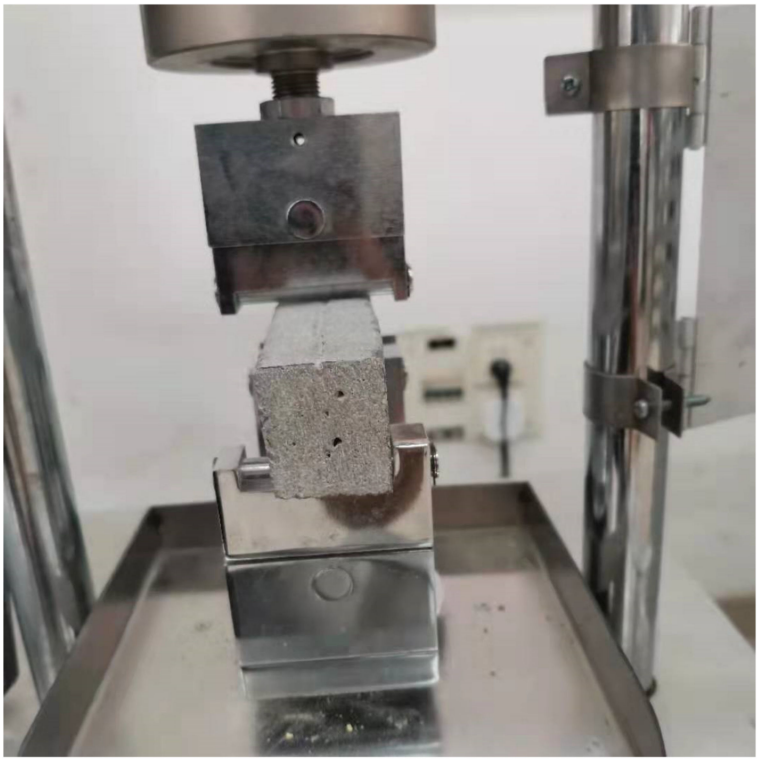


(b) Photograph

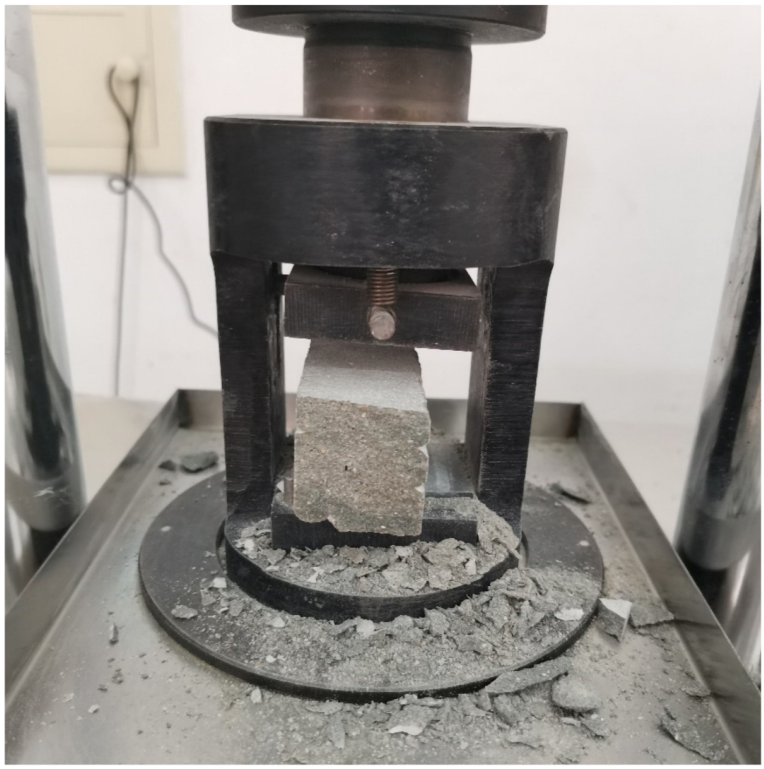
Figure 6. Schematic diagram and photograph of buildability test.



Figure 7. Photograph of 3D printed specimen.



(a) Three-point bending test



(b) Compression test

Figure 8. Photographs of mechanical tests.

Meanwhile, standard prismatic specimens were also cast from the same batch of mortar mixture and cured under the same condition as for the printed specimens until the same age. These standard specimens, produced with no interlayer zones, are called the un-printed specimens. They were also each subjected first to the flexural strength

test and then to the compressive strength test in accordance with Chinese Standard GB/T 17671-1999 [42].

3. Results and Discussions

3.1. SP Dosage and Flow Spread

The optimum SP dosages determined by trial mortar mixing are listed in the second column of Table 2 and plotted against the W/C ratio at different fiber contents in Figure 9.

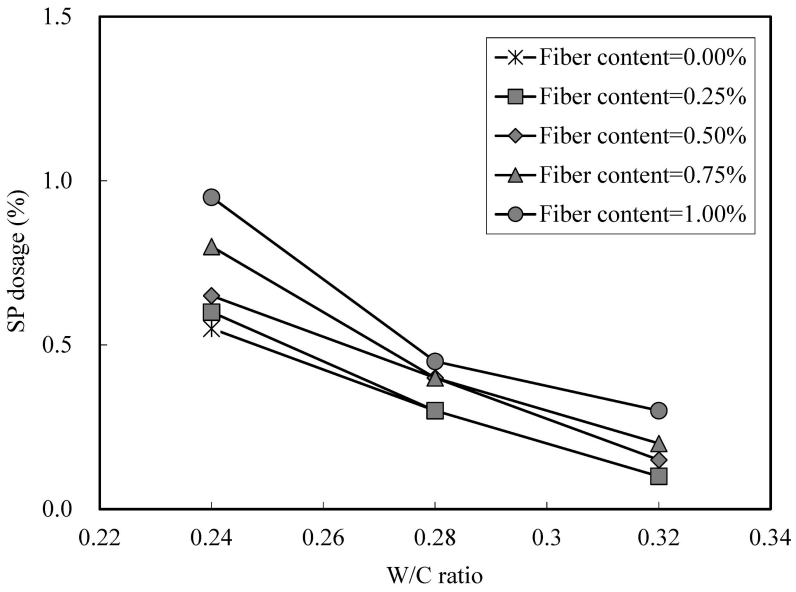


Figure 9. SP dosage vs. W/C ratio at different fiber contents.

As expected, the optimum SP dosage increased as the W/C ratio decreased and/or the fiber content increased. This was because the decreased water content due to the decrease in W/C ratio and the increased fiber entanglement due to the increase in fiber content had both rendered the fresh mortar mix more difficult to flow causing the mortar mixture to require more SP to achieve the target flow spread [43,44]. The corresponding flow spread results are tabulated in the third column of Table 2. It is seen that the flow spread varied from 185 to 218 mm, which is well within the target range.

3.2. Extrudability Variation Coefficient

The extrudability variation coefficient (EVC) results of the printed mortar mixtures are listed in the fourth column of Table 2. From these results, it can be seen that the EVC varied from 1.07% to 2.73%. To graphically depict how the EVC varied, the EVC is plotted against the W/C ratio at different fiber contents in Figure 10.

Generally, at a given fiber content, the EVC increased as the W/C ratio increased, meaning that the increase in water content has a negative impact on the extrudability. This phenomenon is reasonable because with a higher water content, the extruded mortar would be more prone to uncontrolled flow, thus adversely affecting the extrudability [27]. Hence, decreasing the W/C ratio has a positive effect on the extrudability.

Meanwhile, at a fixed W/C ratio, a higher fiber content would generally lead to a lower EVC. For example, at a W/C ratio of 0.24, increasing the fiber content from 0% to 1% reduced the EVC from 2.10% to 1.08%. This indicates that adding glass fibers has a great positive effect on the extrudability. The reason may be that the fiber wrapping would render the extruded mortar more continuous and steadier [27,45].

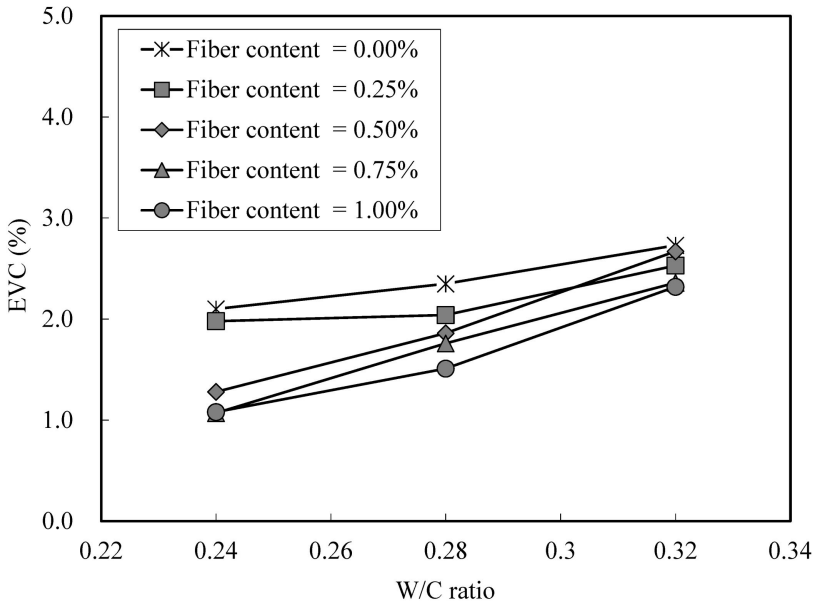


Figure 10. EVC vs. W/C ratio at different fiber contents.

3.3. Dimensional Stability Coefficient

The dimensional stability coefficient (DSC) results of the printed mortar mixtures are exhibited in the fifth column of Table 2. From these results, it can be seen that the DSC varied from 2.94% to 14.29%. To illustrate how the DSC varied, the DSC is plotted against the W/C ratio at different fiber contents in Figure 11.

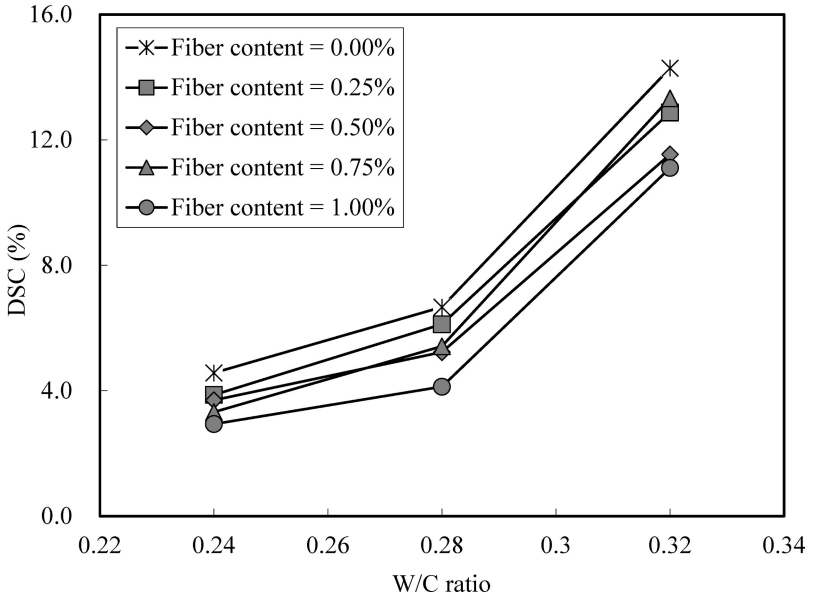


Figure 11. DSC vs. W/C ratio at different fiber contents.

From the figure, it is clear that regardless of the fiber content, as the W/C ratio increased, the DSC also increased, showing that increasing the water content has an adverse effect on the dimensional stability. This phenomenon is expected because adding more water would reduce the cohesiveness of fresh mortar, leading to larger deformation under the weight of the upper layers [25]. Hence, decreasing the W/C ratio has a positive effect on the dimensional stability.

More importantly, at a given W/C ratio, the increase in fiber content would lead to the decrease in DSC. For example, at a W/C ratio of 0.24, when the fiber content increased

from 0% to 1%, the DSC dropped from 4.57% to 2.94%. This means that the addition of glass fibers has a great positive effect on the dimensional stability. The reason for this phenomenon may be that the deformation of mortar in lower layer was inhibited by the wrapping of glass fibers [46,47].

3.4. Buildability Variation Coefficient

The buildability variation coefficient (BVC) results of the printed mortar mixtures, tabulated in the sixth column of Table 2, varied from 0.45% to 1.68%. To graphically display how the BVC changed, the BVC is plotted against the W/C ratio at different fiber contents in Figure 12.

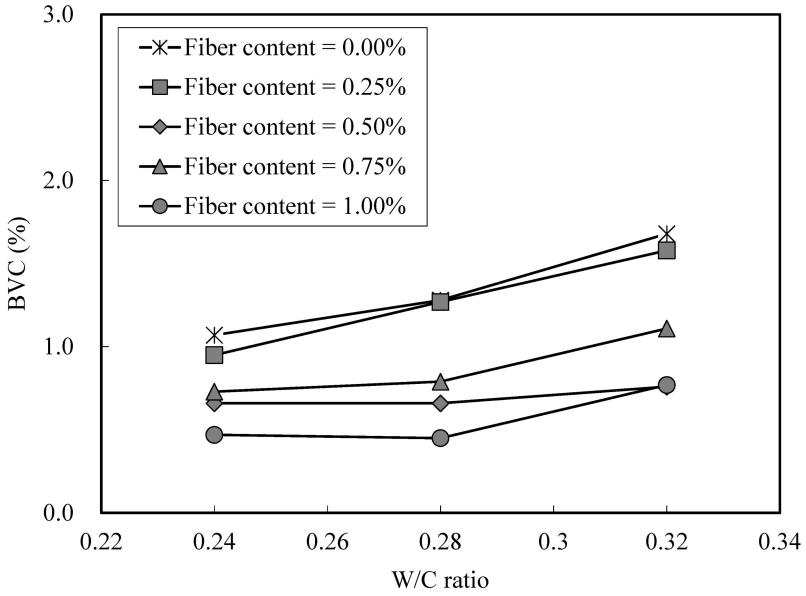


Figure 12. BVC vs. W/C ratio at different fiber contents.

As expected, at a fixed fiber content, the BVC increased with the increase in W/C ratio, meaning that the water added has negative influence on the buildability. This situation is reasonable because as the water content increases, it is more difficult for the printed mortar to hold itself [26]. Hence, decreasing the W/C ratio has a positive effect on the buildability.

More significantly, regardless of W/C ratio, a higher fiber content would generally lead to a lower BVC. For instance, at a W/C ratio of 0.32, when the fiber content increased from 0% to 1%, the BVC decreased from 1.68% to 0.77%. This well confirmed that adding glass fibers has a great positive effect on buildability. This may be due to the fact that the glass fibers played an important part in supporting the printed mortar during the mortar stacking process [25,26].

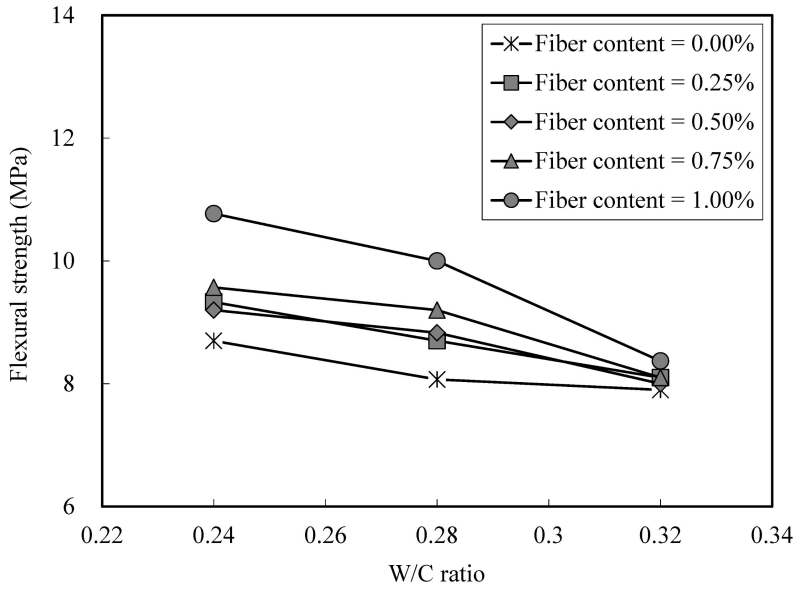
3.5. Flexural Strength

The flexural strength results of the un-printed and printed specimens are tabulated in the second and third columns of Table 3.

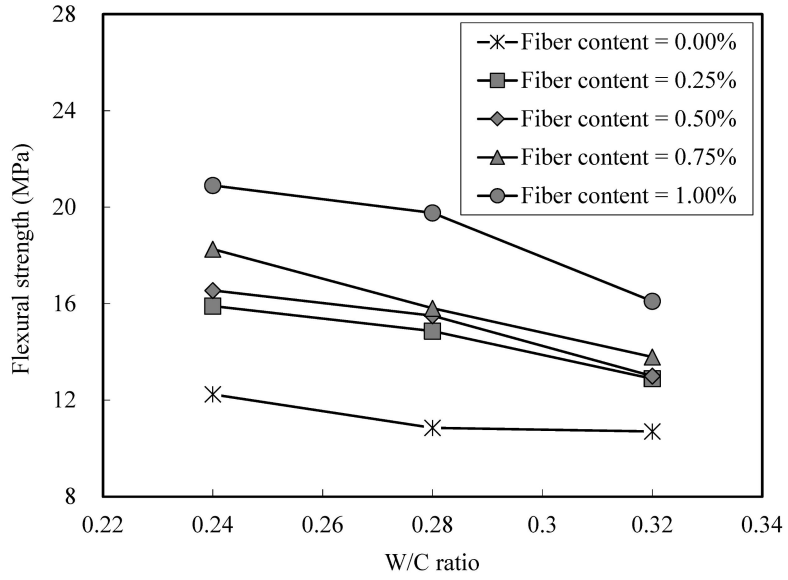
For graphical presentation, the flexural strength results of the un-printed and printed specimens are plotted in Figures 13a and 13b, respectively.

For both the un-printed and printed specimens, at the same fiber content, the flexural strength tended to be higher at lower W/C ratios. This observed effect of the W/C ratio is expected, as it is well known that the W/C ratio is a crucial parameter affecting the strength of cementitious materials and decreasing the W/C ratio would increase the flexural strength [48,49]. For the un-printed specimens, the reduction in the W/C ratio from 0.32 to 0.24 increased the flexural strength from 7.90 to 8.70 MPa by 10.1%. For the printed specimens with 1% fibers added, the reduction in the W/C ratio from 0.32 to 0.24 increased the flexural

strength from 16.10 to 20.90 MPa by 29.8%. Apparently, the percentage increase in flexural strength was higher in the presence of fibers; it was also higher when being printed.



(a) Un-printed specimen

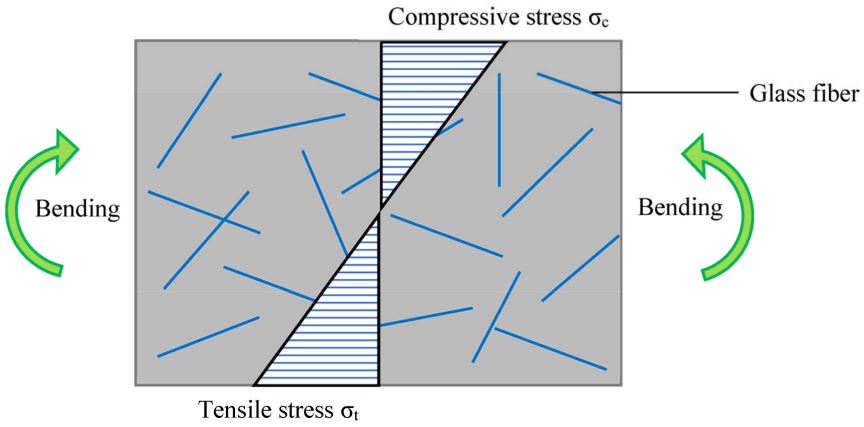


(b) Printed specimen

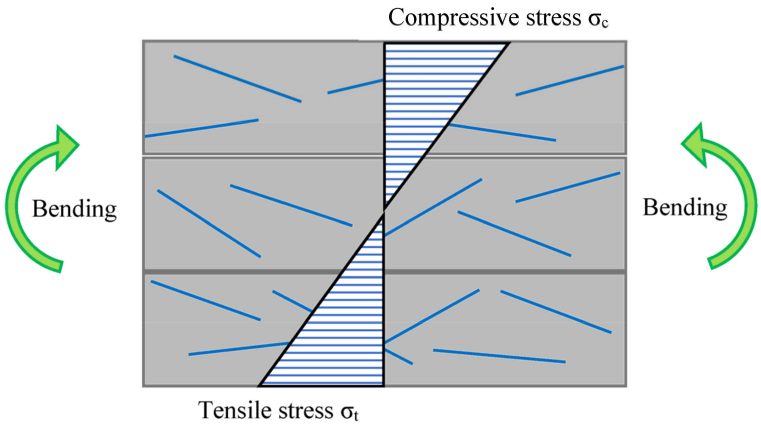
Figure 13. Flexural strength versus W/C ratio at different fiber contents.

On the other hand, for both the un-printed and printed specimens, at the same W/C ratio, the flexural strength always significantly increased with the fiber content. This observed effect of the fiber content is reasonable as the glass fibers would take up part of the tensile stresses and act as tensile reinforcement for bridging cracks to improve the tensile strength of cement-based materials [27,50]. For the un-printed specimens, at a W/C ratio of 0.28, the increase in fiber content from 0% to 1% increased the flexural strength from 8.07 to 10.00 MPa by 23.9%. For the printed specimens, at a W/C ratio of 0.28, the increase in fiber content from 0% to 1% increased the flexural strength from 10.85 to 19.76 MPa by 82.1%. Apparently, the percentage increase in flexural strength was higher when printed.

From the above, it is evident that the printing process, especially the fiber orientation, also has a significant effect. To study its effect, the percentage changes in flexural strength owing to the printing process have been evaluated by comparing the flexural strength of each printed specimen to that of the respective un-printed specimen, as listed in the fourth column of Table 3. These changes were all positive and very substantial indeed. Moreover, the increase in flexural strength was higher at a higher fiber content. For instance, at a fiber content of 0%, the increase due to printing was 34.4% to 40.7%, whereas at a fiber content of 1%, the increase due to printing was 92.4% to 97.6%. It is noteworthy that even with no fibers added, the printing process had increased the flexural strength. Such great differences in flexural strength between the printed and un-printed specimens are the results of material anisotropy caused by the printing process [16–20]. During the printing process, the mortar mixture was squeezed through the nozzle, making the mortar mixture more compact along the printing direction and causing the fibers to be aligned along the printing direction, as shown in Figure 14.



(a) Un-printed specimen



(b) Printed specimen

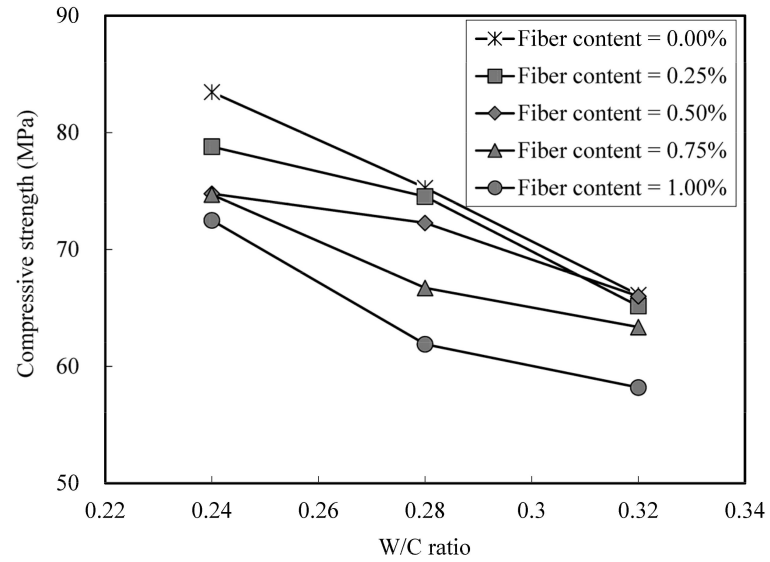
Figure 14. Force diagram of specimen in flexural strength test.

In the flexural strength test, since the tensile stresses induced were along the printing direction, the printed mortar specimens could withstand higher imposed loads. Hence, the beneficial influence of using glass fibers to improve the flexural strength is better manifested after printing.

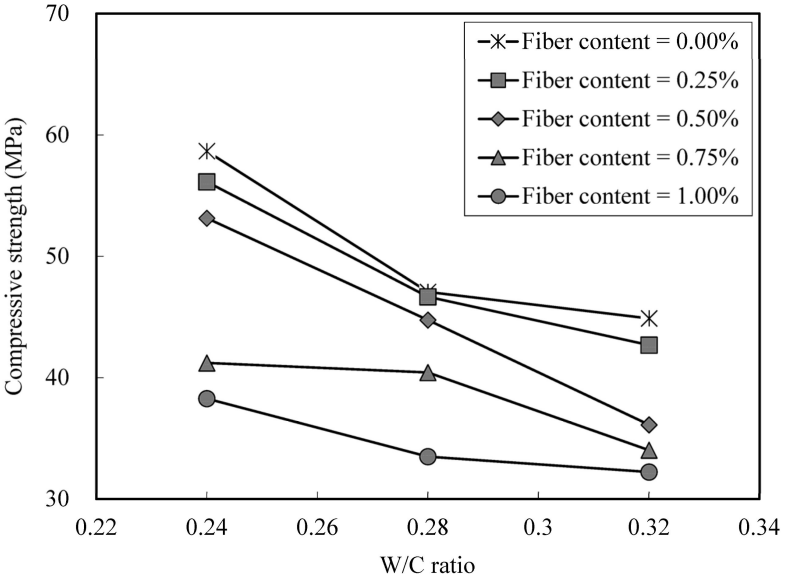
3.6. Compressive Strength

The compressive strength results of the un-printed and printed specimens are tabulated in the second and third columns of Table 4.

To graphically depict how the compressive strength varied, the compressive strength results of the un-printed and printed specimens are plotted in Figures 15a and 15b, respectively.



(a) Un-printed specimen



(b) Printed specimen

Figure 15. Compressive strength versus W/C ratio at different fiber contents.

It is noted that for both the un-printed and printed specimens, at the same fiber content, the compressive strength increased as the W/C ratio decreased. This is a common phenomenon also seen in the compressive strength of other cement-based materials [51–54]. For the un-printed specimens, the reduction in the W/C ratio from 0.32 to 0.24 increased the compressive strength from 66.13 to 83.47 MPa by 26.2%. For the printed specimens with 1% fibers added, the reduction in the W/C ratio from 0.32 to 0.24 increased the compressive strength from 32.23 to 38.28 MPa by 18.8%. Apparently, the percentage increase in compressive strength was lower in the presence of fibers and when printed.

On the other hand, for both the un-printed and printed specimens, at the same W/C ratio, the compressive strength always significantly decreased as the fiber content increased. This observed effect of the fiber content may be explained as follows: adding fibers had rendered the mixing of the fresh mortar harder and caused entanglement of the glass fibers in the mortar mixture and the entrapment of air bubbles, which are detrimental to the compressive strength [55,56]. Similar results had been reported by other researchers [27,50]. In this particular case, for the un-printed specimens, at a W/C ratio of 0.28, the increase in fiber content from 0% to 1% decreased the compressive strength from 75.28 to 61.90 MPa by 17.8%. For the printed specimens, at a W/C ratio of 0.28, the increase in fiber content from 0% to 1% decreased the compressive strength from 47.07 to 33.50 MPa by 28.8%. Apparently, the percentage decrease in compressive strength was higher when printed.

From the above, it is evident that the printing process, especially the fiber orientation, also has a significant effect. To better assess the influence of the printing process, the percentage changes in compressive strength were calculated and listed in the last column of Table 4. These changes were all negative, indicating that the printing process has a negative impact on the compressive strength. Moreover, the decrease in compressive strength was larger at higher fiber contents. For instance, at a fiber content of 0%, the decrease due to printing was 29.7% to 37.5%, whereas at a fiber content of 1%, the decrease due to printing was 44.6% to 47.2%. This detrimental effect may be explained by material anisotropy [11–15] and the presence of porous and weak interlayer zones caused by the printing process [7,18] as shown in Figure 7. In the compressive strength test, the compressive loads acted directly on the porous and weak interlayer zones, making the printed mortar specimens more vulnerable to compressive failure, as shown in Figure 16.

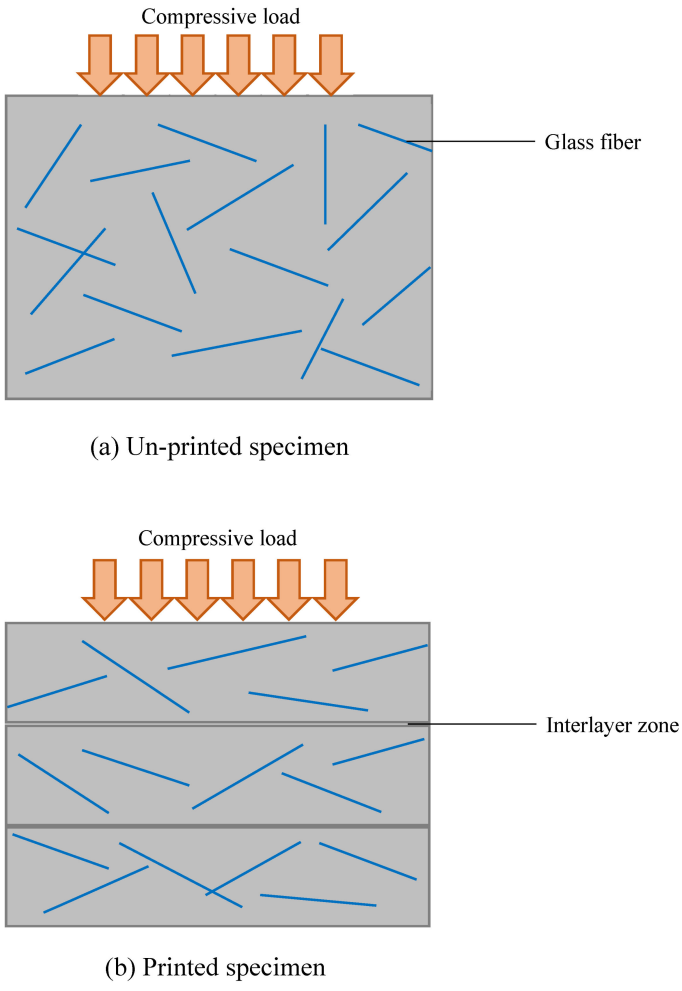


Figure 16. Force diagram of specimen in compressive strength test.

This view is also supported by others [16,57,58]. Such reductions in compressive strength are unavoidable; therefore, for a mortar mixture to be printed, it may be necessary to lower the W/C ratio to compensate for the decline in compressive strength resulting from printing, especially after fibers have been added to improve the printability and flexural strength.

4. Conclusions

A series of 3D printable mortar mixes with different glass fiber contents and water/cement (W/C) ratios, with their SP dosages optimized to attain a certain target fluidity, were designed, made and tested for evaluating their printability and mechanical properties. The conclusions are drawn hereunder:

1. Decreasing the W/C ratio would increase the SP demand, enhance the extrudability, dimensional stability and buildability, and improve the flexural strength and compressive strength.
2. Adding glass fibers would increase the SP demand, but could also substantially improve the extrudability, dimensional stability and buildability of 3D printable mortar, due to wrapping of the glass fibers.
3. An increase in glass fiber content would greatly increase the flexural strength, due to the reinforcing and crack-bridging effects of the glass fibers; but it would also significantly decrease the compressive strength, which is caused by the entanglement of the fibers and the entrapment of air bubbles.
4. The printing process, especially the fiber orientation, has great effects on both the flexural and compressive strengths; it could substantially increase the flexural strength by up to 98% but would also significantly decrease the compressive strength by up to 47%. Such effects are mainly due to the material anisotropy caused by printing and the formation of porous and weak interlayer zones in the printed mortar.
5. To compensate for the decline in compressive strength caused by the printing process, it may be necessary to lower the W/C ratio, especially after fibers have been added, to improve the printability and flexural strength.

Author Contributions: Conceptualization, A.K.H.K.; investigation, B.-F.X. and H.-Z.X.; data curation, B.-F.X.; writing—original draft preparation, B.-F.X.; writing—review and editing, L.G.L., C.-M.C. and A.K.H.K.; supervision, C.-M.C.; project administration, L.G.L.; funding acquisition, L.G.L. All authors have read and agreed to the published version of the manuscript.

Funding: This research was funded by National Natural Science Foundation of China (Project Nos. 51608131), Natural Science Foundation of Guangdong Province (Project No. 2021A1515011747), Science and Technology Planning Project of Guangzhou City (Project No. 2023A03J0088) and Guangzhou University Research Project - Talent Class (Project No. RC2023004).

Data Availability Statement: The data presented in this study are available on request from the corresponding author.

Conflicts of Interest: The authors declare no conflict of interest.

References

1. Wangler, T.; Roussel, N.; Bos, F.P.; Salet, T.A.; Flatt, R.J. Digital concrete: A review. *Cem. Concr. Res.* **2019**, *123*, 105780. [CrossRef]
2. Rahul, A.V.; Santhanam, M.; Meena, H.; Ghani, Z. 3D printable concrete: Mixture design and test methods. *Cem. Concr. Compos.* **2019**, *97*, 13–23. [CrossRef]
3. Khan, M.S.; Sanchez, F.; Zhou, H. 3-D printing of concrete: Beyond horizons. *Cem. Concr. Res.* **2020**, *133*, 106070. [CrossRef]
4. Paolini, A.; Kollmannsberger, S.; Rank, E. Additive manufacturing in construction: A review on processes, applications, and digital planning methods. *Addit. Manuf.* **2019**, *30*, 100894. [CrossRef]
5. Zhang, J.; Wang, J.; Dong, S.; Yu, X.; Han, B. A review of the current progress and application of 3D printed concrete. *Compos. Part A Appl. Sci. Manuf.* **2019**, *125*, 105533. [CrossRef]
6. Xiao, J.; Ji, G.; Zhang, Y.; Ma, G.; Mechtcherine, V.; Pan, J.; Wang, L.; Ding, T.; Duan, Z.; Du, S. Large-scale 3D printing concrete technology: Current status and future opportunities. *Cem. Concr. Compos.* **2021**, *122*, 104115. [CrossRef]

7. Li, L.G.; Xiao, B.F.; Fang, Z.Q.; Xiong, Z.; Chu, S.H.; Kwan, A.K.H. Feasibility of glass/basalt fiber reinforced seawater coral sand mortar for 3D printing. *Addit. Manuf.* **2021**, *37*, 101684. [CrossRef]
8. Chu, S.H.; Li, L.G.; Kwan, A.K.H. Development of extrudable high strength fiber reinforced concrete incorporating nano calcium carbonate. *Addit. Manuf.* **2021**, *37*, 101617. [CrossRef]
9. Wang, L.; Liu, Y.; Yang, Y.; Li, Y.; Bai, M. Bonding performance of 3D printing concrete with self-locking interfaces exposed to compression–shear and compression–splitting stresses. *Addit. Manuf.* **2021**, *42*, 101992. [CrossRef]
10. Nguyen, N.T.; Bui, T.T.; Bui, Q.B. Fiber reinforced concrete for slabs without steel rebar reinforcement: Assessing the feasibility for 3D-printed individual houses. *Case Stud. Constr. Mater.* **2022**, *16*, e00950. [CrossRef]
11. Ding, T.; Xiao, J.; Zou, S.; Zhou, X. Anisotropic behavior in bending of 3D printed concrete reinforced with fibers. *Compos. Struct.* **2020**, *254*, 112808. [CrossRef]
12. Ye, J.; Cui, C.; Yu, J.; Yu, K.; Dong, F. Effect of polyethylene fiber content on workability and mechanical-anisotropic properties of 3D printed ultra-high ductile concrete. *Constr. Build. Mater.* **2021**, *281*, 122586. [CrossRef]
13. Arunothayan, A.R.; Nematollahi, B.; Ranade, R.; Bong, S.H.; Sanjayan, J.G.; Khayat, K.H. Fiber orientation effects on ultra-high performance concrete formed by 3D printing. *Cem. Concr. Res.* **2021**, *143*, 106384. [CrossRef]
14. Singh, A.; Liu, Q.; Xiao, J.; Lyu, Q. Mechanical and macrostructural properties of 3D printed concrete dosed with steel fibers under different loading direction. *Constr. Build. Mater.* **2022**, *323*, 126616. [CrossRef]
15. Guo, Z.S.; Xing, D.; Xi, X.Y.; Yue, X.; Liang, C.G.; Hao, B.; Zheng, Q.; Gutnikov, S.I.; Lazoryak, B.I.; Ma, P.C. Production of fibres from lunar soil: Feasibility, applicability and future perspectives. *Adv. Fiber Mater.* **2022**, *4*, 923–937. [CrossRef]
16. Panda, B.; Paul, S.C.; Tan, M.J. Anisotropic mechanical performance of 3D printed fiber reinforced sustainable construction material. *Mater. Lett.* **2017**, *209*, 146–149. [CrossRef]
17. Ma, G.; Zhang, J.; Wang, L.; Li, Z.; Sun, J. Mechanical characterization of 3D printed anisotropic cementitious material by the electromechanical transducer. *Smart Mater. Struct.* **2018**, *27*, 075036. [CrossRef]
18. Shafighfard, T.; Cender, T.A.; Demir, E. Additive manufacturing of compliance optimized variable stiffness composites through short fiber alignment along curvilinear paths. *Addit. Manuf.* **2021**, *37*, 101728. [CrossRef]
19. Liu, B.; Liu, X.; Li, G.; Geng, S.; Li, Z.; Weng, Y.; Qian, K. Study on anisotropy of 3D printing PVA fiber reinforced concrete using destructive and non-destructive testing methods. *Case Stud. Constr. Mater.* **2022**, *17*, e01519. [CrossRef]
20. Dong, W.; Bao, C.; Lu, W.; Liu, R.; Ma, H.; Li, S.; Sun, K. Fabrication of a continuous carbon fiber-reinforced phenolic resin composites via in situ-curing 3D printing technology. *Compos. Commun.* **2023**, *38*, 101497. [CrossRef]
21. Mohan, M.K.; Rahul, A.V.; Van Tittelboom, K.; De Schutter, G. Rheological and pumping behaviour of 3D printable cementitious materials with varying aggregate content. *Cem. Concr. Res.* **2021**, *139*, 106258. [CrossRef]
22. Tran, M.V.; Cu, Y.T.; Le, C.V. Rheology and shrinkage of concrete using polypropylene fiber for 3D concrete printing. *J. Build. Eng.* **2021**, *44*, 103400. [CrossRef]
23. Jiang, Q.; Liu, Q.; Wu, S.; Zheng, H.; Sun, W. Modification effect of nanosilica and polypropylene fiber for extrusion-based 3D printing concrete: Printability and mechanical anisotropy. *Addit. Manuf.* **2022**, *56*, 102944.
24. Rubio, M.; Sonebi, M.; Amziane, S. 3D printing of fibre cement-based materials: Fresh and rheological performances. *Acad. J. Civ. Eng.* **2017**, *35*, 480–488.
25. Van Der Putten, J.; Rahul, A.V.; De Schutter, G.; Van Tittelboom, K. Development of 3D printable cementitious composites with the incorporation of polypropylene fibers. *Materials* **2021**, *14*, 4474. [CrossRef] [PubMed]
26. Arunothayan, A.R.; Nematollahi, B.; Ranade, R.; Bong, S.H.; Sanjayan, J. Development of 3D-printable ultra-high performance fiber-reinforced concrete for digital construction. *Constr. Build. Mater.* **2020**, *257*, 119546. [CrossRef]
27. Shakor, P.; Nejadi, S.; Sutjipto, S.; Paul, G.; Gowripalan, N. Effects of deposition velocity in the presence/absence of E6-glass fibre on extrusion-based 3D printed mortar. *Addit. Manuf.* **2020**, *32*, 101069. [CrossRef]
28. Weng, Y.; Lu, B.; Li, M.; Liu, Z.; Tan, M.J.; Qian, S. Empirical models to predict rheological properties of fiber reinforced cementitious composites for 3D printing. *Constr. Build. Mater.* **2018**, *189*, 676–685. [CrossRef]
29. Madhkhan, M.; Katirai, R. Effect of pozzolanic materials on mechanical properties and aging of glass fiber reinforced concrete. *Constr. Build. Mater.* **2019**, *225*, 146–158. [CrossRef]
30. Xue, G.; Yilmaz, E.; Song, W.; Cao, S. Analysis of internal structure behavior of fiber reinforced cement-tailings matrix composites through X-ray computed tomography. *Compos. Part B Eng.* **2019**, *175*, 107091. [CrossRef]
31. Tibebu, A.; Mekonnen, E.; Kumar, L.; Chimdi, J.; Hailu, H.; Fikadu, N. Compression and workability behavior of chopped glass fiber reinforced concrete. *Mater. Today Proc.* **2022**, *62*, 5087–5094. [CrossRef]
32. Jin, Y.; Zhou, X.; Chen, M.; Zhao, Z.; Huang, Y.; Zhao, P.; Lu, L. High toughness 3D printed white Portland cement-based materials with glass fiber textile. *Mater. Lett.* **2022**, *309*, 131381. [CrossRef]
33. *GB 175-2020*; Common Portland Cement. General Administration of Quality Supervision, Inspection and Quarantine of the People's Republic of China: Beijing, China, 2020. (In Chinese)
34. Tay, Y.W.D.; Qian, Y.; Tan, M.J. Printability region for 3D concrete printing using slump and slump flow test. *Compos. Part B Eng.* **2019**, *174*, 106968. [CrossRef]
35. *GB/T 2419-2005*; Test Method for Fluidity of Cement Mortar. General Administration of Quality Supervision Inspection and Quarantine of the People's Republic of China: Beijing, China, 2005. (In Chinese)

36. Chen, Y.; Li, Z.; Chaves Figueiredo, S.; Çopuroğlu, O.; Veer, F.; Schlangen, E. Limestone and calcined clay-based sustainable cementitious materials for 3D concrete printing: A fundamental study of extrudability and early-age strength development. *Appl. Sci.* **2019**, *9*, 1809. [CrossRef]
37. Panda, B.; Unluer, C.; Tan, M.J. Investigation of the rheology and strength of geopolymer mixtures for extrusion-based 3D printing. *Cem. Concr. Compos.* **2018**, *94*, 307–314. [CrossRef]
38. Le, T.T.; Austin, S.A.; Lim, S.; Buswell, R.A.; Gibb, A.G.F.; Thorpe, T. Mix design and fresh properties for high-performance printing concrete. *Mater. Struct.* **2012**, *45*, 1221–1232. [CrossRef]
39. Kazemian, A.; Yuan, X.; Cochran, E.; Khoshnevis, B. Cementitious materials for construction-scale 3D printing: Laboratory testing of fresh printing mixture. *Constr. Build. Mater.* **2017**, *145*, 639–647. [CrossRef]
40. Zhang, Y.; Zhang, Y.; Liu, G.; Yang, Y.; Wu, M.; Pang, B. Fresh properties of a novel 3D printing concrete ink. *Constr. Build. Mater.* **2018**, *174*, 263–271. [CrossRef]
41. Wolfs, R.J.M.; Bos, F.P.; Salet, T.A.M. Early age mechanical behaviour of 3D printed concrete: Numerical modelling and experimental testing. *Cem. Concr. Res.* **2018**, *106*, 103–116. [CrossRef]
42. *GB/T 17671-1999*; Method of Testing Cements—Determination of Strength. General Administration of Quality Supervision, Inspection and Quarantine of the People's Republic of China: Beijing, China, 1999. (In Chinese)
43. Mazloom, M.; Soltani, A.; Karamloo, M.; Hassanloo, A.; Ranjbar, A. Effects of silica fume, superplasticizer dosage and type of superplasticizer on the properties of normal and self-compacting concrete. *Adv. Mater. Res.* **2018**, *7*, 45.
44. Zhang, K.; Pan, L.; Li, J.; Lin, C. What is the mechanism of the fiber effect on the rheological behavior of cement paste with polycarboxylate superplasticizer? *Constr. Build. Mater.* **2021**, *281*, 122542. [CrossRef]
45. Luhar, S.; Suntharalingam, T.; Navaratnam, S.; Luhar, I.; Thamboo, J.; Poologanathan, K.; Gatheeshgar, P. Sustainable and renewable bio-based natural fibres and its application for 3D printed concrete: A review. *Sustainability* **2020**, *12*, 10485. [CrossRef]
46. Ogura, H.; Nerella, V.N.; Mechtcherine, V. Developing and testing of strain-hardening cement-based composites (SHCC) in the context of 3D-printing. *Materials* **2018**, *11*, 1375. [CrossRef] [PubMed]
47. Zhou, W.; Zhang, Y.; Ma, L.; Li, V.C. Influence of printing parameters on 3D printing engineered cementitious composites (3DP-ECC). *Cem. Concr. Compos.* **2022**, *130*, 104562. [CrossRef]
48. Atiş, C.D.; Celik, O.N. Relation between abrasion resistance and flexural strength of high volume fly ash concrete. *Mater. Struct.* **2002**, *35*, 257–260. [CrossRef]
49. Oad, M.; Buller, A.H.; Memon, B.A.; Memon, N.A.; Tunio, Z.A.; Memon, M.A. Effect of water-cement ratio on flexural strength of RC beams made with partial replacement of coarse aggregates with coarse aggregates from old concrete. *Eng. Technol. Appl. Sci. Res.* **2019**, *9*, 3826–3831. [CrossRef]
50. Yoo, D.-Y.; Zi, G.; Kang, S.-T.; Yoon, Y.-S. Biaxial flexural behavior of ultra-high-performance fiber-reinforced concrete with different fiber lengths and placement methods. *Cem. Concr. Compos.* **2015**, *63*, 51–66. [CrossRef]
51. Chidiac, S.E.; Panesar, D.K. Evolution of mechanical properties of concrete containing ground granulated blast furnace slag and effects on the scaling resistance test at 28 days. *Cem. Concr. Compos.* **2008**, *30*, 63–71. [CrossRef]
52. Wang, Q.; Wang, D.; Zhuang, S. The soundness of steel slag with different free CaO and MgO contents. *Constr. Build. Mater.* **2017**, *151*, 138–146. [CrossRef]
53. Li, L.G.; Ng, P.L.; Zeng, K.L.; Xie, H.Z.; Cheng, C.M.; Kwan, A.K.H. Experimental Study and Modelling of Fresh Behaviours of Basalt Fibre-Reinforced Mortar Based on Average Water Film Thickness and Fibre Factor. *Materials* **2023**, *16*, 2137. [CrossRef]
54. Zheng, Y.; Zhou, Y.; Huang, X.; Luo, H. Effect of raw materials and proportion on mechanical properties of magnesium phosphate cement. *J. Road Eng.* **2022**, *2*, 243–251. [CrossRef]
55. Li, L.G.; Zhuo, H.X.; Zhu, J.; Kwan, A.K.H. Packing density of mortar containing polypropylene, carbon or basalt fibres under dry and wet conditions. *Powder Technol.* **2019**, *342*, 433–440. [CrossRef]
56. Chu, S.H.; Jiang, Y.; Kwan, A.K.H. Effect of rigid fibres on aggregate packing. *Constr. Build. Mater.* **2019**, *224*, 326–335. [CrossRef]
57. Pham, L.; Tran, P.; Sanjayan, J. Steel fibres reinforced 3D printed concrete: Influence of fibre sizes on mechanical performance. *Constr. Build. Mater.* **2020**, *250*, 118785. [CrossRef]
58. Nematollahi, B.; Vijay, P.; Sanjayan, J.; Nazari, A.; Xia, M.; Naidu Nerella, V.; Mechtcherine, V. Effect of polypropylene fibre addition on properties of geopolymers made by 3D printing for digital construction. *Materials* **2018**, *11*, 2352. [CrossRef]

Disclaimer/Publisher's Note: The statements, opinions and data contained in all publications are solely those of the individual author(s) and contributor(s) and not of MDPI and/or the editor(s). MDPI and/or the editor(s) disclaim responsibility for any injury to people or property resulting from any ideas, methods, instructions or products referred to in the content.